Journal of Experimental and Theoretical Physics, Vol. 95, No. 1, 2002, pp. 154–165.
Translated from Zhurnal Éksperimental'noĭ i Teoreticheskoĭ Fiziki, Vol. 122, No. 1, 2002, pp. 175–187.

MISCELLANEOUS

Diffusion in Smooth Hamiltonian Systems

V. V. Vecheslavov* and B. V. Chirikov**

Budker Institute of Nuclear Physics, Siberian Division, Russian Academy of Sciences, pr. Akademika Lavrent'eva 11, Novosibirsk, 630090 Russia

**e-mail: vecheslavov@inp.nsk.ru*

***e-mail: chirikov@inp.nsk.ru*

Received September 6, 2001

Abstract—A family of models determined by a smooth canonical 2D-map that depends on two parameters is studied. Preliminary results of numerical experiments are reported; they are evidence of substantial suppression of global diffusion in a wide range of perturbation values. This effect is caused by the little-known phenomenon of the conservation of resonance separatrices and other invariant curves under the conditions of strong local dynamic chaos. Such a total suppression of diffusion occurs although invariant curves are only conserved for a countable zero-measure set of parameter values. Simple refined estimates of diffusion rates in smooth systems without invariant curves were obtained and numerically substantiated. The principal boundary of diffusion suppression in a family of models with invariant curves was described by a semiempirical equation in dimensionless variables. The results were subjected to a statistical analysis, and an integral distribution for diffusion suppression probability was obtained. © *2002 MAIK "Nauka/Interperiodica".*

1. INTRODUCTION

One of the principal concepts of the modern theory of nonlinear Hamiltonian systems is the assertion that splitting of a nonlinear resonance separatrix and the formation of a chaotic layer in its place in a typical (that is, nonintegrable) system occurs under an almost arbitrary perturbation. It is also believed that precisely separatrices are destroyed first, because the period of motion along them is infinite, and the interaction of nonlinear resonances in their vicinity is always substantial (e.g., see [1–4]). Invariant curves (surfaces) experience breakup and disappear as perturbation increases. This as a rule causes overlapping of chaotic layers of all resonances and the appearance of so-called "global" chaos.

The conditions of global chaos formation and the possibility of diffusion over the whole unified chaotic component in the phase space depend not only on the value but also on the smoothness of perturbation. The smoothness can conveniently be characterized by the rate of decreasing Fourier amplitudes. An analytic perturbation decreases exponentially, and a threshold perturbation value ε_{tr} always exists. Global diffusion only arises at $\varepsilon \gtrsim \varepsilon_{tr}$. If $\varepsilon < \varepsilon_{tr}$, chaos is localized in comparatively narrow chaotic layers (which are formed at arbitrary $\varepsilon > 0$ values), and there can be no global diffusion in a conservative system with the number of degrees of freedom $\mathcal{N} \le 2$.

Note that, if $\mathcal{N} > 2$, global diffusion can only take place under special initial conditions (Arnold diffusion, e.g., see [1]). The rate of this diffusion and the measure of its region decrease exponentially with respect to the $1/\varepsilon$ parameter as $\varepsilon \longrightarrow 0$.

The character of motion changes considerably for a smooth perturbation of the Hamiltonian whose Fourier amplitudes decrease as some power $\beta + 1$ of their number n (e.g., see [5] and the references therein). In the simplest case of a 2D map, to which our analysis will be restricted, the $\varepsilon_{tr} > 0$ threshold of the appearance of global chaos always exists if $\beta > \beta_{cr} = 3$. This critical smoothness value was obtained from the simple estimate made in [5] (also see Section 3), but it nevertheless requires verification by numerical experiments. So far as we know, a rigorous proof can only be obtained for $\beta_{cr} = 5$ (see [6], where the suggestion is made that, in reality, $\beta_{cr} = 4$). This uncertainty is of no significance for our purposes, because, for the model under consideration (Section 2), the inequality $\beta = 2 < \beta_{cr}$ is always satisfied. Interestingly, the situation has long remained unclear precisely for the $\beta = 2$ index.

Even in early numerical experiments on systems whose smoothness was lower than critical, trajectories that did not go beyond some limited phase space region in long-time computations were observed along with global diffusion [7, 8]. This was, however, nothing more than a suspicion of diffusion suppression or weakening. A rigorous result was obtained by Bullett [9], who proved the existence of global invariant curves with both irrational and rational rotation numbers for a symmetrical piecewise linear 2D map [$\beta = 2$—see (2.1) and (2.2) below; also see [10] and Section 2]. Precisely global invariant curves have a complete phase extent, which prevents unlimited diffusion over action. In [9], it was found for the first time that, among invariant curves with rational rotation numbers, there are also (at special perturbation parameter values) intact nonlinear

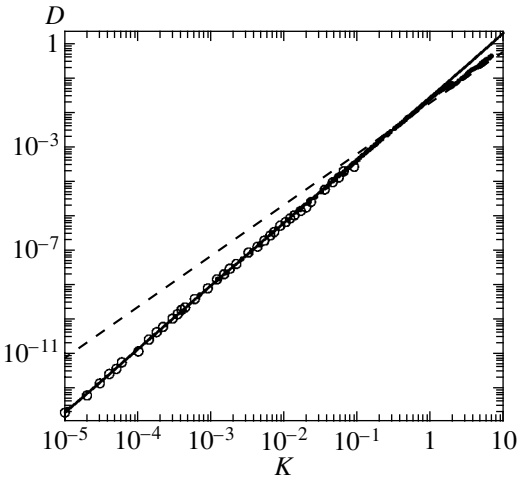

Fig. 1. Diffusion rate $D(K)$ in model (2.2) with the $d = 0$ parameter (without invariant curves): dots are the data from [17], open circles are our data averaged over 250 trajectories $t_0 = 4 \times 10^7$ iterations long with random initial conditions, solid line is power dependence (4.1), and dashed line is limiting mode (3.10).

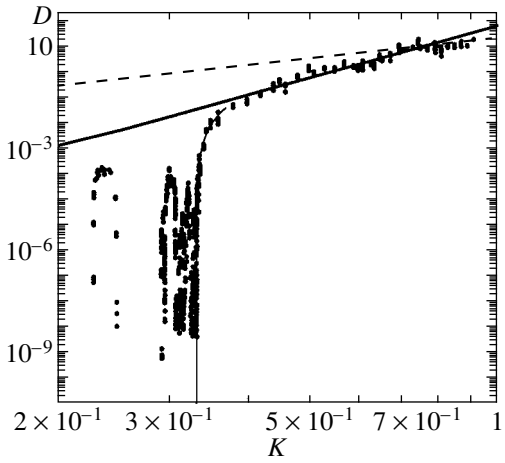

Fig. 2. Example of diffusion in a smooth map with invariant curves of measure zero: model (2.2) with the $d = 1/2$ parameter, 50 trajectories, computation time $t_0 = 2.5 \times 10^6$. The solid straight line is $D_2 = 0.8K^5$ according to (5.1), and the dashed line is limiting mode (3.10).

resonance separatrices. Especially important and unexpected was that the system nevertheless remained nonintegrable, but the separatrix not only was conserved under strong chaos conditions but also prevented global diffusion.

A similar theorem for the same model was later proved by Ovsyannikov [11], who not only specified a countable set of parameter values at which the separatrix of an integer resonance is conserved but also found an explicit and very simple expression for the separatrix. Although Ovsyannikov proved his theorem independently, such a coincidence of the models was not fortuitous, because solving a linear (even though piecewise) map considerably simplifies the problem. Note that completely solving even a linear map is only possible if the separatrix is conserved, because otherwise two branches of a split separatrix form random trajectories. For the same reason, a symmetrical piecewise linear 2D map cannot be simplified to a purely linear map of the type of the Arnold map, in which nonlinear resonance separatrices are always split. The mathematical works by Bullett and Ovsyannikov are therefore restricted to studies of only new-type invariant curves themselves. The first examples of such curves were predicted in [10].

Precisely the Ovsyannikov theorem prompted us to thoroughly study the symmetrical piecewise linear 2D map and its modifications [12–15]. Unfortunately, this theorem was not published by its author (the complete formulation of the theorem can be found in Appendix in [14]). Instead, the theorem was generalized in [16] to arbitrary map parameter values. The result obtained in [16] contradicts that of [9] and our numerical experiment data.

A certain perturbation parameter value corresponds to each invariant curve in the symmetrical piecewise linear 2D map (including invariant curves of the new type with rational rotation numbers, that is, also integer and fractional resonance separatrices). The set of all such values is a Cantor set (see Figs. 2 and 3 in [9]), and there are intervals of parameter values in which global diffusion certainly takes place (one of such intervals is identified in [9]; also see Section 5). As the density of this set is fairly high, we can expect strong (although incomplete) suppression of global diffusion at an arbitrary perturbation parameter value. Studies in this direction were performed in the present work.

2. MODEL

The selected model is a two-dimensional map in the canonical variables of action p and phase x,

$$\bar{p} = p + Kf(x), \quad \bar{x} = x + \bar{p} \mod 1. \tag{2.1}$$

Here, $K = \varepsilon > 0$ is the perturbation parameter (not necessarily small), and "force" $f(x)$ has the form of an antisymmetric [$f(-y) = -f(y)$, $y = x - 1/2$] piecewise linear "saw" with period 1.

We will study the whole family of sawtooth perturbations[1] (see Fig. 1 in [15]),

$$f(x) = \begin{cases} \dfrac{2x}{1-d}, & \text{for } |x| \le \dfrac{1-d}{2}, \\ -\dfrac{2y}{d}, & \text{for } |y| \le \dfrac{d}{2}, \end{cases} \tag{2.2}$$

[1] A family similar but not identical to that of the model used in [9].

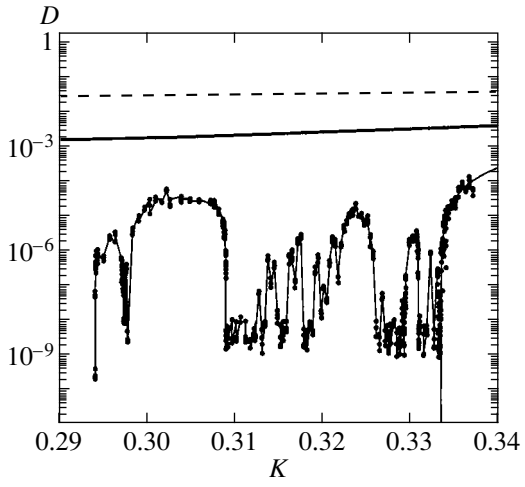

Fig. 3. Part of fractal diffusion region extended along K with invariant curves shown in Fig. 2. The computation parameters are the same as in Fig. 2 except that $t_0 = 4 \times 10^7$ for most of the points. For some points, including the leftmost with $K = 0.294$, computation time $t_0 = 10^9$. The smooth curve at the right was constructed by (5.5); it approximates the boundary of the principal diffusion region.

where $y = x - 1/2$, and $0 \le d \le 1$ is the distance between saw "teeth" $|f(x)| = 1$ situated at the points $y = y_\pm = \pm d/2$. The most thoroughly studied particular case of the symmetrical piecewise linear 2D map corresponds to the bias parameter $d = 1/2$.

We are interested in global diffusion over momentum, which is suppressed by invariant curves with a complete extent over phase. We call these invariant curves global and, in what follows, only consider such curves unless otherwise stated. Note that these invariant curves (including unbroken separatrices of integer and fractional resonances) exist for an arbitrary bias parameter value in the interval $0 < d < 1$ at special K values [9, 12–15].

If $0 < d < 1$, force (2.2) can be written as the Fourier series

$$f(x) = \sum_{n \ge 1} \frac{f_n}{n^\beta} \sin(2\pi n x), \tag{2.3}$$

where

$$f_n = -\frac{2}{\pi^2} \frac{\cos(n\pi)\sin(n\pi d)}{d(1-d)}, \quad \beta = 2. \tag{2.4}$$

The passage to the $d \longrightarrow 0$ limit in (2.3) and (2.4) for the discontinuous saw yields

$$f_n = -\frac{2}{\pi} \cos(n\pi), \quad \beta = 1. \tag{2.5}$$

One can see that, in the $d = 0$ limit, the smoothness index of the system, β, is smaller by one than within the interval, and both indices are smaller than the $\beta_{cr} = 3$ critical value. The second $d \longrightarrow 1$ limit is not considered in this work, because motion then becomes regular (see [15]).

Map (2.1) can be written as a continuous system with a Hamiltonian that explicitly depends on time and perturbation in the form of impulses [1–3, 14]:

$$H(x, p, t) = \frac{p^2}{2} + K \sum_{n \ge 1} \frac{f_n}{2\pi n^{\beta+1}} \cos(2\pi n x) \delta_1(t), \tag{2.6}$$

where

$$\delta_1(t) = 1 + 2 \sum_{m \ge 1} \cos(2\pi m t)$$

denotes the δ function with period 1. Note that selecting the δ function in this form also defines the time unit of the continuous system; this unit equals one iteration of the initial map.

Each term of the double sum in (2.6) is proportional to $\cos[2\pi(nx - mt)]$ with integer m and n and determines "its own" primary nonlinear resonance (details are given, e.g., in [1]). Supposing that these resonances do not interact with each other, we can describe any of them by the Hamiltonian of a "pendulum"

$$H_{nm}(x, p, t) = \frac{p^2}{2} + \frac{K f_n}{2\pi n^{\beta+1}} \cos[2\pi(nx - mt)]. \tag{2.7}$$

Introducing the resonance momentum value $p_{nm} = \dot{x}_{nm} = m/n$, we find that, in the new variables $\tilde{x} = nx - mt$ and $\tilde{p} = (p - p_{nm})/n$, each such solitary resonance is a conservative system with motion strictly bounded with respect to momentum. Returning to the old variables, we determine the frequency of phase oscillations

$$\Omega_n^2 = \frac{2\pi K f_n}{n^{\beta-1}} \tag{2.8}$$

and the total momentum width of the resonance

$$(\delta p)_n = 4\sqrt{\frac{K f_n}{2\pi n^{\beta+1}}}. \tag{2.9}$$

In the next section, these equations are used to obtain very simple and unexpectedly accurate estimates of the rate of diffusion for a smooth map without invariant curves.

3. DIFFUSION RATE ESTIMATES

Our estimates are based on the criterion of overlapping of nonlinear resonances (see [1–3, 5]), which can be written in the simplest form as

$$\mathcal{P} \sim 1, \tag{3.1}$$

where

$$\mathcal{P} \sim \sum_{n \geq 1} n(\delta p)_n = 4\sqrt{\frac{Kf_0}{2\pi}}\mathcal{S}, \qquad \mathcal{S} = \sum_{n \geq 1} n^{(1-\beta)/2}. \tag{3.2}$$

Here, $\mathcal{P}$ is the approximate sum of widths (2.9) of all primary resonances in a unit interval with respect to momentum p. For simplicity, we assume that all Fourier coefficients are equal, $f_n = f_0$.

Note that the sum diverges at $\beta \leq 3$, and this determines the critical smoothness value specified above, $\beta_{cr} = 3$, in the approximation that we use. Global diffusion then occurs at an arbitrary K value, including $K \longrightarrow 0$, and, generally, its rate depends on all resonances (2.7) and is described by complex and cumbersome equations (cf. [17]). As in [5], our simple estimates are based on the following hypothesis, which we consider physically plausible and which is substantiated by the numerical experiments described below. We assume that the mean rate of global diffusion at $\beta \leq 3$ is largely determined by a finite number of resonances up to some critical harmonic $n = n_c$. These resonances, in combination with various m values in (2.7), provide overlapping (3.1). Indeed, stronger resonances ($n < n_c$) cause faster diffusion, but this diffusion is local because of incomplete overlapping of resonances. On the other hand, weaker resonances ($n > n_c$) more than provide overlapping, but the rate of diffusion for them

$$D = \frac{\overline{(\delta p)^2}}{t} \sim \frac{(\delta p)_n^2 \Omega_n}{2\pi} \tag{3.3}$$

rapidly decreases as n increases. Here, the total resonance width (2.9) and the period of the corresponding phase oscillations $2\pi/\Omega_n$ [see (2.8)] are used as dynamic diffusion scales.

Replacing the sum in (3.2) by the integral in $n \gg 1$ yields

$$\mathcal{S} \approx \frac{2}{3-\beta} n^{(3-\beta)/2}. \tag{3.4}$$

It follows from (3.2) that the number of the critical harmonic is

$$n_c \sim \left[\frac{\pi}{32}\frac{(3-\beta)^2}{Kf_0}\right]^{1/(3-\beta)}. \tag{3.5}$$

Lastly, (3.3) is used to obtain the rate of diffusion,

$$D_{\beta<3}(K) \sim \frac{4\sqrt{2\pi}}{\pi^2} \times \left(\frac{32}{\pi(3-\beta)^2}\right)^{(3\beta+1)/2(3-\beta)} (Kf_0)^{5/(3-\beta)}. \tag{3.6}$$

Generally, this equation only gives an estimate of the order of magnitude. We, however, deliberately leave various numerical coefficients in it in the hope that its accuracy can be substantially increased through the introduction of empirical correction factors. This will be done in the next section in considering a simple and thoroughly studied example of such diffusion.

Note that all these estimates are only valid at $K \ll 1$. Indeed, as mentioned, diffusion in the system under consideration has two dynamic scales,

$$(\delta p)_c \sim 4\sqrt{\frac{Kf_0}{2\pi n_c^{\beta+1}}} \sim K^{2/(3-\beta)} \lesssim 1 \tag{3.7}$$

with respect to momentum (2.9) and

$$t_c \sim \sqrt{\frac{2\pi n_c^{\beta-1}}{Kf_0}} \sim K^{-1/(3-\beta)} \gtrsim 1 \tag{3.8}$$

with respect to time [from (2.8)]. Both scales are bounded because p is periodic and t discrete. This imposes the limitation on the system parameter

$$K \lesssim 1. \tag{3.9}$$

The same limitation arises also from the condition imposed on critical harmonic (3.5), namely, $n_c \gtrsim 1$. At $K \ll 1$, the time of the decay of perturbation correlations satisfies the inequality $t_c \gg 1$. At $K \sim 1$, this time is shortened to $t_c \sim 1$, and at $K \gg 1$, correlations between closely spaced impulses become negligibly small. The rate of diffusion is then determined by the mean square perturbation,

$$D_{K\to\infty} = K^2 \int_0^1 f^2(x)dx = \frac{K^2}{3}, \tag{3.10}$$

and ceases to depend on bias parameter d for the whole family of maps (2.1), (2.2).

4. NUMERICAL EXPERIMENTS FOR A MODEL WITHOUT INVARIANT CURVES

First, consider the simplest example of a smooth 2D map, which corresponds to the $d = 0$ parameter in family (2.2). According to [15], invariant curves are absent in this limiting case, and global diffusion occurs at arbitrary positive $K > 0$. Diffusion in such a model was thoroughly studied numerically and analytically fairly long ago [17]. Note that both the diffusion rate and perturbation parameter K are normalized differently in [17] and this work, and the data obtained in [17] and cited below were therefore recalculated to our model.

Substituting $\beta = 1$ and $f_0 = 2/\pi$ [see (2.5)] into (3.6) yields $D_{\beta=1}(K) = 0.84K^{2.5}$. Recalculating the value numerically obtained in [17] yields

$$D_1(K) = A_1 K^{B_1} = C_D D_{\beta=1}(K),$$
$$A_1 = 0.5680 \pm 0.0034, \quad (4.1)$$
$$B_1 = 2.4940 \pm 0.008,$$

where the correction factor for the diffusion rate $C_D = 0.68$. In what follows, we use the assumption made by the authors of [17], namely, $B_1 = 2.5$, for comparison with their theory.

The C_D correction to our theoretical estimate is small, but it heavily depends on the smoothness index β. By way of example, we set $\beta = 2$. Equation (3.6) gives $D_{\beta=2}(K) = 1199K^5$ against the numerical calculation result $D_2(K) \approx 0.8K^5$ [see (5.1) and Fig. 2]. A comparison of these values gives a correction factor $C_D \approx 6.7 \times 10^{-4}$ (!), which makes this factor physically meaningless.

Physically unreasonable results are obtained because the principal approximation for constructing estimates is related to an intermediate result in the formulation of the condition of resonance overlapping, Eqs. (3.1) and (3.2), rather than directly to diffusion rate D. In such a form, this condition always overestimates the overlapping effect because it contains maximum widths of resonance separatrices, whereas, in reality, separatrices may have mutual phase shifts. This circumstance can be taken into account by introducing correction C_s in place of C_D,

$$\mathcal{P} = C_s > 1. \quad (4.2)$$

C_s is essentially different from C_D in (4.1) because it is raised to some power, which depends on β and can be fairly large,

$$D_{\beta<3}(K) \approx \frac{4\sqrt{2\pi}}{\pi^2} \times \left(\frac{32}{\pi(3-\beta)^2 C_s^2}\right)^{(3\beta+1)/2(3-\beta)} (K f_0)^{5/(3-\beta)}. \quad (4.3)$$

To obtain $C_D \approx 1$ for $\beta = 2$ (see above), it suffices to set $C_s \approx 2.84$ [see (5.1)]. This is evidence that such a method for introducing an empirical correction into order-of-magnitude estimates is very effective.

The C_s correction is much smaller for $\beta = 1$, $C_s \approx 1.2$, because the perturbation spectrum at $\beta = 1$ contains all harmonics, whereas only odd harmonics remain at $\beta = 2$. As a result, sum (3.2) decreases twofold. This additional effect is easy to take into account in (4.3) by the replacement $C_s \longrightarrow 2C_s$. The necessary correction for $\beta = 2$ then decreases from 2.84 to 1.42, which is close to the $C_s \approx 1.2$ value found above for $\beta = 1$.

The most important results obtained in studying the simple model with $d = 0$ and the approximating straight line found in [17] [Eq. (4.1)] are shown in Fig. 1. This straight line is also fairly well described by our simple theory (4.3) with correction $C_s = 1.2$. Both equations closely agree with the empirical data up to the $K \sim 1$ value, at which the transition to mode (3.10) occurs.

Numerical data were compared in [17] with a very complex theory developed by the authors, which was also based on the concept of overlapping of resonances (more exactly, of their destroyed separatrices). This theory did not include adjustment parameters of any kind, but the accuracy that it provided was in reality not high (approximately 10%, see Fig. 2 in [17]). The theory actually referred to a qualitatively different model with an analytic Hamiltonian with a finite number of harmonics n retained in its Fourier transform. Such a "cutting off" of the spectrum was accompanied by the appearance of a threshold for the arising of global diffusion, as is characteristic of analytic systems, which limited the applicability of this theory to the most interesting region of small parameter K values, $K \lesssim K_c(n)$. In the example given in [17] (see Fig. 2 in [17]), $n_c = 21$ and $K_c \sim 0.02$ (in our normalization). The mechanism of this limitation resembles that of restriction (3.5) imposed on the critical harmonic in our theory, but our restriction is much weaker. For instance, at $n_c = 21$ and $C_s = 1.2$, the minimum value is

$$K \approx K_c(n_c) \approx \left(\frac{\pi C_s}{4n_c}\right)^2 \approx 0.002, \quad (4.4)$$

which is one order of magnitude smaller than in [17].

We turn to the most interesting part of our study, when the bias parameter of model (2.2) is $d \neq 0$. It has been proved in [9] that there exists a critical perturbation parameter value K_B such that, at $K > K_B$, there is no global invariant curves in the system. The exact equation for K_B in our normalization takes the form

$$K_B(d) = \frac{2d^2}{1+d}, \quad 0 < d < 1. \quad (4.5)$$

According to [9–15], generally, there is a countable set of special $K \leq K_B$ values at which invariant curves are formed in the system under strong local chaos conditions.

Our main interest is how strongly the existence of these invariant curves suppresses global diffusion at arbitrary K values, although the measure of the set of special K values and the probability of fortuitously falling into it are zero.

5. DIFFUSION SUPPRESSION BY "VIRTUAL" INVARIANT CURVES

First consider the most thoroughly studied example of family (2.2) with the bias parameter $d = 1/2$, for which the results of our numerical experiments are shown in Figs. 2 and 3.

In the computations, the whole time interval was divided into four equal portions, and the diffusion rate was output at the end of each interval. For this reason, four points generally correspond to each K value in

Figs. 2–5. Their arrangement along vertical lines allows the diffusive case to be distinguished from the nondiffusive one. Characteristic of the latter is a decrease in the rate of diffusion in time, which results in mutual "dispersal" of these points. The spread of points for diffusion characterizes the accuracy of diffusion rate values. In the region without invariant curves, this accuracy is quite satisfactory (approximately 10%), as for $d = 0$. However, in the region with virtual invariant curves and in its vicinity (at $K \sim K_B$), the error increases and sometimes reaches 2. Of the same order is a systematic decrease in the mean diffusion rate caused by nonergodicity of motion in this region. Nonergodicity of motion results in the formation of a stable motion component of a very complex structure (so-called critical structure, e.g., see [5]). Currently, we have not been able to substantially increase the accuracy of determining the rate of diffusion. However, we believe the attained accuracy to be sufficient for our purposes.

The $d = 1/2$ value is the only one (except the $d = 0$ limiting value) when the $|f_n| = \text{const}$ simplification in (3.2) is possible. This simplification substantially facilitates a theoretical analysis of numerical data. By virtue of this simplification, Eq. (4.3) with $|f_n| = 8/\pi^2$ is applicable to odd harmonics, and the same equation with $|f_n| = 0$, to even harmonics at $\beta = 2$ with correction $C_s = 2.84$ [see (2.4) and the preceding section], but only in the region without invariant curves. In addition, (4.3) is only valid in a very limited range of perturbation parameter values (see Fig. 2), namely,

$$D_2(K) = 0.8K^5, \quad 0.4 \lesssim K \lesssim 0.8. \tag{5.1}$$

The upper bound is determined by the well-known transition to the limiting diffusion conditions without correlations (3.10). An essentially new feature of the diffusion picture is the lower bound, clearly related to the appearance of invariant curves, which suppress diffusion. According to (4.5), invariant curves at $d = 1/2$ are completely absent if

$$K > K_B\left(\frac{1}{2}\right) = \frac{1}{3}. \tag{5.2}$$

It is, however, obvious from Figs. 2 and 3 that strong diffusion suppression begins much earlier, that is, in the region of K values where invariant curves are actually absent! Hence our new term "virtual invariant curve." In other words, every real invariant curve, which is formed at some strictly definite special $K = K_0$ value, in reality substantially distorts the structure of the phase plane of the system in some finite neighborhood of K_0.

Diffusion in the vicinity of a single invariant curve in system (2.2) with $d = 1/2$, in the vicinity of an undestroyed integer resonance separatrix formed at $K = K_0 = 1/8$, was for the first time studied in [13]. The first thing observed was sharp asymmetry at $K > K_0$ and $K < K_0$.

At $K > K_0$, the separatrix begins to transmit other trajectories, but the mean time (the number of iterations) T_c of passing the resonance depends on the detuning $K - K_0 > 0$. The following measurements were preformed to determine this dependence in the interval $1.25 \times 10^{-7} \le K - K_0 \le 1.25 \times 10^{-5}$, where there was no other invariant curves. In the region between two neighboring integer resonances (see Fig. 4 in [13]), 100 random chaotic trajectories were generated, and time T_c of the first appearance of each of them in the region either below the lower or above the higher resonance was fixed. To facilitate comparison of these data with the results of the present work, we give the equation for the diffusion rate

$$D_c(K) \approx \frac{1}{\langle T_c \rangle} = 0.089(K - K_0)^{1.193}, \quad K > K_0 = \frac{1}{8}. \tag{5.3}$$

The $F_{\text{ex}} = D_2(K)/D_c(K)$ ratio, where, according to (5.1), $D_2(K)$ determines the diffusion rate on the assumption of the complete absence of invariant curves in the system, is the quantitative measure of diffusion suppression. For instance, in the whole $K - K_0$ range that we studied, this coefficient changed from 40 000 to 200, which was evidence of substantial diffusion suppression (also see Figs. 2 and 3).

Note beforehand that (5.3) is in a certain way similar to Eq. (5.5) for the boundary of the principal diffusion region; this similarity is discussed below.

At $K < K_0$ and in the region arbitrarily close to the separatrix, many closely spaced invariant curves were observed; because of their presence, the problem of determining the resonance passage time was virtually unsolvable. The question of diffusion in this region remains open.

All these fairly simple observations are, we believe, most important at the same time, because they show that the zero measure of the set of invariant curves and even their finite density do not prevent strong diffusion suppression in the model under consideration.

The next important problem is that of quantitatively estimating diffusion suppression. Complete diffusion suppression is likely to be possible only at special K_0 values, that is, only for real invariant curves. Generally, everything depends on their structure in the space of system parameters (K, d). This structure appears to be fairly complex and is likely to be fractal. In particular, it also includes whole regions of finite width without invariant curves. One of such regions, $0.2295 < K < 0.2500$, has been predicted in [9] and is well seen at the left of Fig. 2. The rate of diffusion rapidly decreases at the boundaries of this region, as at the principal boundary $K = 1/3$ (5.2). This causes diffusion suppression

Parameters of diffusion regions shown in Fig. 3

K_{max}	D_{max}	F_{ex}	C_F	$\Delta K \times 100$	$\delta K \times 100$
0.3322	9.9×10^{-7}	3.26×10^{3}	1.99×10^{0}	0.080	0.051
0.3309	4.0×10^{-6}	7.93×10^{2}	1.30×10^{0}	0.155	0.130
0.3282	1.0×10^{-8}	3.05×10^{5}	1.20×10^{2}	0.060	0.003
0.3270	5.0×10^{-8}	5.98×10^{4}	1.85×10^{1}	0.051	0.007
0.3240	1.1×10^{-5}	2.60×10^{2}	1.65×10^{0}	0.382	0.274
0.3216	2.0×10^{-6}	1.38×10^{3}	1.15×10^{0}	0.099	0.090
0.3204	1.0×10^{-7}	2.70×10^{4}	5.58×10^{0}	0.039	0.012
0.3196	8.0×10^{-7}	3.34×10^{3}	1.73×10^{0}	0.072	0.050
0.3178	2.0×10^{-6}	1.30×10^{3}	4.01×10^{-1}	0.051	0.094
0.3163	1.0×10^{-6}	2.53×10^{3}	1.84×10^{0}	0.090	0.060
0.3146	4.0×10^{-7}	6.16×10^{3}	1.58×10^{0}	0.045	0.033
0.3139	8.0×10^{-7}	3.05×10^{3}	7.81×10^{-1}	0.045	0.053
0.3130	5.0×10^{-8}	4.81×10^{4}	2.04×10^{1}	0.063	0.008
0.3043	4.0×10^{-5}	5.22×10^{1}	1.59×10^{0}	1.090	0.798
0.2978	3.0×10^{-7}	6.25×10^{3}	4.05×10^{-1}	0.018	0.033
0.2960	2.5×10^{-6}	7.27×10^{2}	3.22×10^{0}	0.301	0.138
0.2941	4.3×10^{-7}	4.06×10^{3}	2.00×10^{-1}	0.0150	0.044

Note: K_{max} and D_{max} are the perturbation parameter and the rate of diffusion in the center of the region, respectively; F_{ex} is the experimental diffusion suppression factor in the center of the region; $C_F = F_{ex}/F_{th}$ is the ratio between the experimental and theoretical suppression factors; F_{th} is calculated by (5.6); ΔK is the experimental region width; and δK is the region width recalculated by (5.5) under the additional requirement of providing the $C_F \equiv 1$ equality.

even at the maximum. The width of this region is $\Delta K \approx 0.02$, and the diffusion suppression factor is

$$F_{ex} = \frac{D_2(K_{max})}{D_{max}} \approx 14. \quad (5.4)$$

Here, $D_{max} \approx 4.6 \times 10^{-5}$ is the maximum measured diffusion rate near the center of the region $K_{max} \approx 0.24$, and $D_2(K_{max}) \approx 6.4 \times 10^{-4}$ is the diffusion rate expected in the complete absence of invariant curves in the system, Eq. (5.1).

A crude estimate of F_{ex} can be made by comparing the boundary of this region and the $D_B(K)$ principal boundary, which, according to Fig. 2, is satisfactorily approximated by the equation (to the left of the arrow)

$$D_B(K) \approx \frac{1}{2}\left(K - \frac{1}{3}\right)^{3/2} \longrightarrow D_b(K) \approx \frac{1}{2}(K - K_b)^{3/2}. \quad (5.5)$$

This particular case substantiates the natural suggestion that the K_B critical value from (4.5), which is the boundary value for the principal region without invariant curves, coincides with K_D (or is close to it) at the $D_B(K_D) = 0$ boundary of the principal diffusion region.

In addition, we make the suggestion (which should also be verified) that the boundaries of all diffusion regions exhibit similar behaviors, and Eq. (5.5) to the right of the arrow is therefore applicable to an arbitrary region without invariant curves with the K_b left boundary.

Equation (5.5) yields

$$F_{th} \approx \frac{2D_2(1/3)}{D_b(K_{max})} \approx 13. \quad (5.6)$$

Here, coefficient 2 characterizes interference of two region boundaries, which amplifies diffusion suppression; $K_b \approx 0.23$ and $K_{max} \approx 0.24$ are the left boundary and the center of the region under consideration, and $D_b(K_{max}) \approx 5 \times 10^{-4}$ is the rate of diffusion in the center obtained from Eq. (5.5) for the boundary. Lastly, $D_2(1/3) \approx 3.28 \times 10^{-3}$ is the diffusion rate at the boundary of the principal region calculated by (5.1) on the assumption of the absence of invariant curves (we ignore the small $K_{max} - K_b$ correction and use $K = 1/3$).

For the model under consideration, the measured (5.4) and theoretical (5.6) values very closely agree with each other, which substantiates the suggestion made above that diffusion region boundaries are similar. By analogy with (4.1), we may introduce an empirical correction factor $G_F = F_{ex}/F_{th} \approx 1.1$, which is close to one. Note that approximation (5.5) is only valid for $d = 1/2$ (see below), and applying it to narrow diffusion

regions appears to be justified only in the vicinity of the principal boundary.

We stress once more that dependence (5.3) for diffusion rate $D_c(K)$ close to one invariant curve and dependence (5.5) for the $D_B(K)$ boundary of the principal region are similar; not only both are power dependences but also their exponents differ insignificantly. This difference is likely to arise because (5.3) is calculated at $K = 1/8$ and (5.5), at $K = 1/3$.

Several other narrower diffusion regions are also shown in Fig. 2. They are reproduced in Fig. 3 on an enlarged scale. The empirical values are connected by a polygonal line, which helps us to distinguish between closely spaced narrow regions. In the centers of these regions without invariant curves, diffusion is also suppressed the stronger, the narrower the region. For 17 regions that we were able to discern, calculations by (5.4)–(5.6), similar to those made above, were performed. These data are summarized in the table, which also contains the $C_F = F_{ex}/F_{th}$ empirical correction factors. Given in the last column are region widths calculated by (5.5) under the additional requirement to provide fulfillment of the equality $C_F \equiv 1$. For the widths, agreement with empirical estimates is much worse, which appears to be caused by difficulties of determining the width of a narrow ΔK region based on a limited number of perturbation parameter K values used in the calculations (see below).

Diffusion suppression at several bias parameter d values is shown in Fig. 4. Similarity of $D(K)$ dependences at different d values attracts attention. This similarity gives promise that a unified description of diffusion in some dimensionless variables can be constructed.

On the assumption that $K_D \approx K_B$ (see above), it is natural to write dimensionless perturbation parameter K^* as

$$K^* = \frac{K}{K_B} = \frac{1+d}{2d^2}K. \tag{5.7}$$

The determination of the second dimensionless variable D^* involves serious difficulties because, generally, $|f_n| \neq \text{const}$ (see Section 3) and an explicit expression for the $D(K)$ function cannot therefore be obtained. This function can, however, be described approximately if the argument of the sine function in (2.4) is small. We then have $\sin(\pi nd) \approx \pi nd$ and [see (2.3)]

$$|f_n| \approx n f_0, \quad f_0 \approx \frac{2}{\pi}, \quad \beta = 1. \tag{5.8}$$

Clearly, the $D(K)$ dependence at $d \ll 1$ is the same as in the $d = 0$ limit.

This approximation [and, therefore, asymptotic equation (4.1)] is valid at [see (3.5) with $\beta = 1$]

$$K \gtrsim K_1 = \frac{\pi^4 d^2}{16} \approx \frac{\pi^4}{32}K_B \approx 3K_B. \tag{5.9}$$

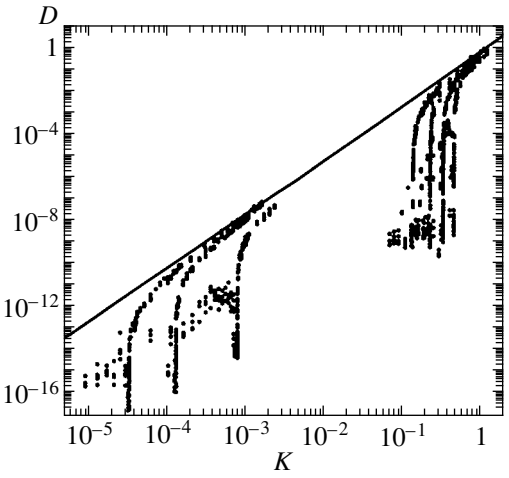

Fig. 4. General picture of diffusion in model (2.2) at seven bias parameter d values, $d = 0.004$, 0.008, 0.02, 0.3, 0.4, 0.5, and 0.6 (from left to right). The number of trajectories 50–250, computation time $t_0 = 2.5 \times 10^6$ iterations. The straight line is the upper bound of diffusion rate (4.1); also see text and Fig. 5.

On the other hand, if the inverse inequality holds ($\pi n_c d \gtrsim 1$, $d \ll 1$, $\beta = 2$), $\sin(\pi nd)$ in (2.4) can be averaged over n. As the sum in (3.2) satisfies the proportionality relation

$$\sqrt{f_n} \propto \sqrt{|\sin(\pi nd)|},$$

we can introduce the new parameter

$$S_0 = \langle \sqrt{|\sin(\pi nd)|} \rangle \approx 0.76 \tag{5.10}$$

and set ($d \ll 1$)

$$f_0 \approx \frac{2}{\pi^2}\frac{S_0^2}{d}, \quad \beta = 2. \tag{5.11}$$

The averaging condition can also be written as

$$K \lesssim K_2 \approx \left(\frac{\pi^2 d}{8S_0}\right)^2 \approx 2.6d^2 \approx 1.3K_B < K_1. \tag{5.12}$$

We then have

$$D(K) \approx A_2 K^5, \quad A_2 \approx \frac{A_1}{K_{cr}^{2.5}}, \tag{5.13}$$

where the A_1 value is taken from (4.1), and K_{cr} is the intersection point between two asymptotic dependences, (5.13) and (4.1). The position of this point is not known, and it is not clear how it can be determined, because, at $d \ll 1$ (as distinguished from the case of $d = 1/2$ in Fig. 2), there is no diffusion region with $\beta = 2$. At the same time, both K_1 and K_2 boundaries are fairly close to K_B. For this reason, the abscissa of the intersec-

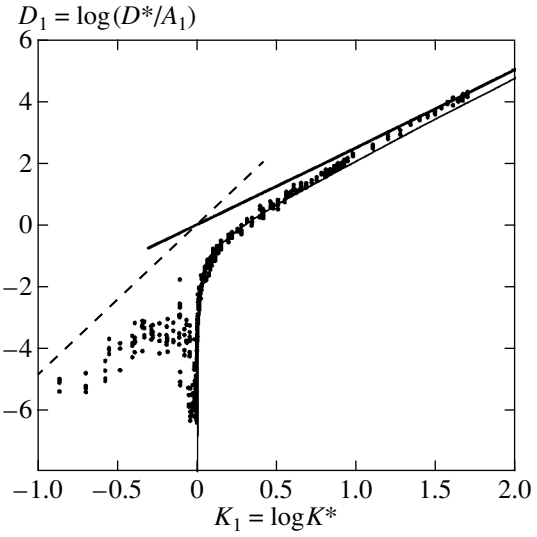

Fig. 5. General picture of diffusion in model (2.2) for the three smallest d parameter values, d = 0.004, 0.008, and 0.02, in dimensionless variables (5.7) and (5.15). The curve is the empirical approximation of the principal boundary of diffusion (5.16). The straight lines describe asymptotic behaviors of diffusion without invariant curves: the solid line corresponds to (4.1) with $\beta = 1$, and the dashed line, to (5.13) with $\beta = 2$ in approximation (5.14).

tion point between the two asymptotic dependences can be assumed to be

$$K_{cr} \approx K_B. \tag{5.14}$$

In this approximation and taking into account (5.7) and (5.13), the second dimensionless variable can be selected in the form

$$D^* = \left(\frac{1+d}{2d^2}\right)^{5/2} D. \tag{5.15}$$

Strictly, variables (5.7) and (5.15) are suitable only if $d \ll 1$, when simple asymptotic dependences (4.1) and (5.13) can be used. The general similarity picture, however, persists to $d \sim 1$, but not for $d \longrightarrow 1$.

The results of our numerical experiments for $d \ll 1$ are shown in dimensionless variables in Fig. 5 together with two asymptotic dependences (4.1) and (5.13). The smooth curve, which can with difficulty be traced in the dense system of points, corresponds to the purely empirical universal boundary of the principal diffusion region found by us,

$$\begin{gathered} D_l = \frac{5}{2}K_l - \frac{0.4}{\sqrt{K_l}}, \\ D_l = \log\left(\frac{D^*}{A_1}\right), \quad K_l = \log K^*, \end{gathered} \tag{5.16}$$

which is written in the decimal logarithms of dimensionless variables.

This equation contains dimensionless variables (4.5) and (5.15), in which the suggestion of the equality of the K_B critical number and the K_D boundary of the principal diffusion region is implicit. Preliminary experiments (see Figs. 3–5) confirm this suggestion to high accuracy,

$$\frac{K_D - K_B}{K_B} \leqslant 10^{-3}.$$

The interesting question of exact equality of these two parameters, however, remains open.

In [9], only one region without invariant curves was found (see above), and the suggestion was made that the number of such regions grew infinitely as $K \longrightarrow 0$. Our results (Fig. 3) show that a set of such regions also exists in the immediate vicinity of the principal diffusion boundary. An important problem is the statistics of such regions related to the distribution of diffusion rates with respect to perturbation parameter K and, accordingly, to its suppression by virtual invariant curves.

We performed a statistical treatment of the experimental diffusion suppression coefficients F_{ex} for N = 134 parameter K values in the interval $0.293 < K < 0.333$ of width as small as $\Delta \approx 0.04$ (see Fig. 3). An effective method for obtaining a statistically significant distribution $P(F_{ex})$ for such poor statistics is the special method for constructing an integral distribution with a "floating" cell width (see [18] and the references therein). This method is also called "rank-ordering statistics of extreme events." This effective procedure was for the first time suggested in 1949 and used in mathematical linguistics [19]. It turns out that it suffices to arrange all $F_{ex}(n)$, $n = 1, 2, \ldots, N$ values in decreasing order, $F_{ex}(n+1) < F_{ex}(n)$. The sought distribution is then given by the approximate equality

$$P(F_{ex}) \approx \frac{n}{N}, \quad n = 1, 2, \ldots, N. \tag{5.17}$$

The distribution obtained in this simple way is shown in Fig. 6. Its most interesting feature is an exceedingly slow decrease in the probability of strong diffusion suppression,

$$\begin{gathered} P(F_{ex}) \approx \frac{2}{F_{ex}^{0.15}}, \\ 100 < F_{ex} < 3 \times 10^5 = F_{max}(t_0). \end{gathered} \tag{5.18}$$

Here, the left boundary is related to the very narrow interval of K values used in the calculations, $\Delta \approx 0.04$. The rapid decrease in probability $P(F_{ex})$ at $F_{ex} > 3 \times 10^5$ is explained by the limited time of calculations ($t_0 = 4 \times 10^7$). Indeed, as regular oscillations $\Delta p \sim K \approx 0.3$, the minimum observed diffusion rate is given by

$$D_{min} \sim \frac{(\Delta p)^2}{t_0} \sim 10^{-9}, \tag{5.19}$$

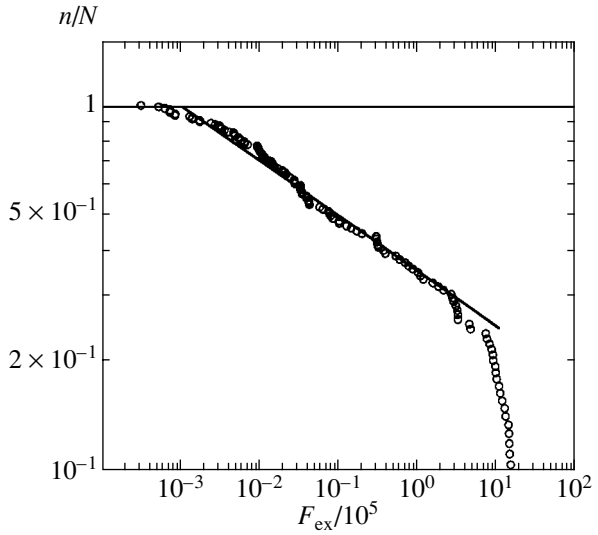

Fig. 6. The first empirical results on the statistic of the F_{ex} factor (5.4) of diffusion suppression by virtual invariant curves according to our numerical experiments shown in Fig. 3 (d = 1/2). The slanted straight line corresponds to integral power distribution (5.18). The total number of F_{ex} values is 134; 100 of them lie within the principal interval $F_{ex} < 3 \times 10^5$ (see text).

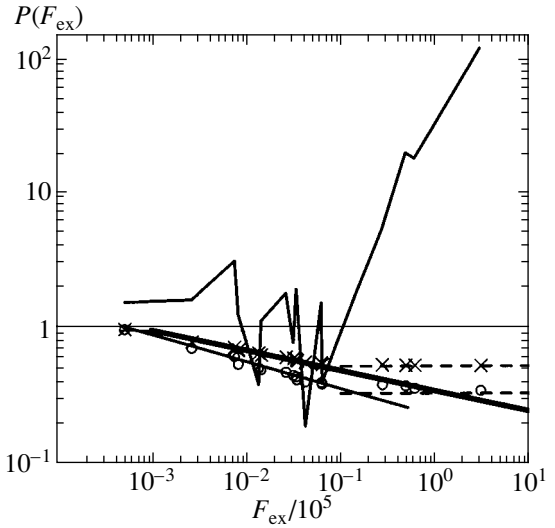

Fig. 7. The same as in Fig. 6 but over the width of 17 discernible diffusion regions (see table and text). Thick line corresponds to the data from Fig. 6 (5.18), circles are integral probabilities (5.21) determined from the experimental ΔK width of diffusion regions, crosses are integral probabilities for the δK width recalculated by (5.5), polygonal line is the experimental C_F correction to (5.6), and dashed horizontal lines are the fractions of "lost" (indiscernible) regions at large $F \gtrsim 10^4$.

which closely agrees with the experimental data shown in Fig. 3. At smaller K values, this minimum decreases even to $D \approx 10^{-17}$ at $K \approx 3 \times 10^{-5}$, $t_0 = 4 \times 10^8$ (see Fig. 4). Interestingly, at such a slow decrease in probability (5.18), both the mean F_{ex} value and its variance are determined by the F_{max} value and diverge approximately proportionally to $t_0 \longrightarrow \infty$ [see (5.19)].

Small deviations of the empirical distribution shown in Fig. 6 from law (5.18) are likely to be related to nonuniformities of the K_n values used in the calculations. This may easily be corrected, but will require considerable computation time or a substantial statistical reduction.

Empirical law (5.18) can, in particular, be used to analyze enigmatic trajectory "jamming" observed in old work [7], which still remains unexplained. This phenomenon is also related to map (2.2) with d = 1/2, but in a somewhat different normalization, as in [9]. In the notation that we use, it corresponds to $K = 0.29 <$ 1/3 and, therefore, it fortuitously falls into the region with invariant curves. At a $t_0 = 3 \times 10^6$ time of computations, the minimum diffusion coefficient is $D_{min} \sim 3 \times 10^{-8}$, which corresponds to the minimum diffusion suppression factor $F_{min} \sim 10^5$ with a reasonable probability $P \approx 36\%$.

Instead of separate $F_{ex}(n)$ values, we can take the F_m values [here, the notation is simplified: F_m stands for $F_{ex}(m)$] for the centers of all m = 1, 2, …, M (M = 17) discernible in the K = 0.293–0.333 selected interval of diffusion regions (see table). The probability is then proportional to the normalized sum of the widths of these regions dK_m, which are found either empirically from Fig. 3 (ΔK in the table) or by recalculation according to (5.5) from the empirical suppression factor F_m value (δK in the table). The normalization is performed with respect to the total width of the K interval as $dK_m \longrightarrow dK_m/\Delta$, where Δ = 0.04. In addition, it should be taken into account that the normalized sum of the widths of all M = 17 diffusion regions is $S \approx 0.664$ for ΔK and $S \approx 0.468$ for δK. In both cases, significant loss of narrow regions with large $F \gtrsim 10^4$ occurs (see Fig. 7). We eventually obtain

$$P(F_m) \approx 1 - S + \sum_{i=m}^{M} dK_i. \qquad (5.20)$$

The result of such a processing of the empirical data summarized in the table is shown in Fig. 7 together with the data from Fig. 6, which are plotted by a thick line corresponding to (5.18). Agreement for such limited statistics can be considered satisfactory. This especially refers to the δK data (within the $F \lesssim 10^4$ limitation introduced above). Note that outside this region, that is, at $F \gtrsim 10^4$, where the $P(F)$ probability is almost constant, we simultaneously observe a sharp increase in the C_F empirical correction (see Fig. 7).

Agreement is worse for ΔK, and we observe not only spread of data but also a systematic although small deviation. As previously, the empirical distribution remains a power function (see the lowest slanted

straight line in Fig. 7) but with a somewhat different exponent,

$$P(F) \approx \frac{2.3}{F^{0.20}}, \quad 64 < F \lesssim 10^4, \tag{5.21}$$

where the left boundary is determined by the minimum F value in the studied K range. The reason for these discrepancies is not known and requires further inquiries. We suggest that the observed discrepancies are largely caused by underestimation of the empirical width of the ΔK region, which increases as F grows. This in all probability occurs as a result of overlapping of neighboring regions, which also increases with F. The difference between empirical equations (5.18) and (5.21) amounts to about 30% in the exponent and 20% in the probability [within the range of the applicability of (5.21)], which is not bad for preliminary results.

Note that diffusion rate fluctuations mentioned above (not exceeding twofold rate changes) change probability (5.18) by a factor of $2^{0.15} \approx 1.11$; that is, by as little as 11%.

6. CONCLUSION

Studies of a family of piecewise linear maps of types (2.1) and (2.2) have a long history (e.g., see [7, 9, 11–15, 17] and the references therein). In this work, we use very simple models to study a comparatively new and little-known but very complex phenomenon of fractal diffusion under the action of virtual global invariant curves and under the conditions of strong local chaos.

However, first, it would be useful to understand why studies of such simplified constructions as piecewise linear maps deserve attention. Let us return to work [17], where a complex analytic function with 21 Fourier harmonics was used to study the properties of such a map, and a certain similarity between the dynamic behaviors of this function and the map was observed. We can therefore use the opposite approach and, for a complex continuous analytic function, for instance, for a function with sharp turns, seek a piecewise linear function close to the analytic function and study the corresponding map, which is much simpler. This approach, we believe, offers much promise, but requires special consideration.

Our studies show that, in the family of models (2.1), (2.2), there always exists a comparatively wide (principal) region of "normal" diffusion, as in other smooth systems without invariant curves. We were able to obtain fairly simple and fairly accurate diffusion rate estimates in this region (Sections 3 and 4), which were of considerable help in analyzing the most important empirical data on fractal diffusion in the region with virtual invariant curves (Section 5).

Our studies were performed in the range of bias parameter values $0 < d < 0.6$ [with invariant curves at $K < K_B$, see (4.5)]. We found that the presence of a set of invariant curves, although of measure zero, caused strong diffusion suppression at $K < K_B$, which prompted us to suggest a new term, namely, "virtual invariant curve."

The case of $d = 1/2$ was studied most thoroughly. For this case, we were able to obtain quantitative estimates of diffusion suppression. Preliminary treatment of empirical data allowed us to construct integral distribution (5.18) for the probability of the F_{ex} diffusion suppression coefficient. The most interesting feature of this distribution was an exceedingly slow decrease in the probability of F_{ex}, slow to the extent that the mean F_{ex} value diverged as the time of computations increased (see Section 5). We also thoroughly studied a series of narrow diffusion regions to the left of the principal boundary (see table). This also allowed us to substantiate important result (5.18) by another method [see (5.21)]. The reason for such unusual statistics of F_{ex} [and, therefore, of the rate of fractal diffusion D_{max} in (5.4)] is not known and requires further inquiries.

Studies of the $D(K)$ dependences at different d values revealed obvious similarity of their behavior, which was an indication that their universal description might be possible. We were able to give such a description on the additional assumption that $d \ll 1$ and construct empirical dependence (5.16) for the boundary of the principal diffusion region in dimensionless variables. This simple dependence fairly well described the characteristic sharp transition from the chaotic region without invariant curves with well-known regular diffusion to an also chaotic region but with a dense system of invariant curves of a new form with absolutely unknown very irregular (fractal) diffusion.

On the whole, we consider this new phenomenon fairly interesting and important; in our view, it deserves further investigation.

ACKNOWLEDGMENTS

This work was financially supported by the Russian Foundation for Basic Research (project no. 01-02-16836) and by the Russian Academy of Sciences ("Nonlinear dynamics and solitons" Program).

REFERENCES

1. B. V. Chirikov, Phys. Rep. **52**, 263 (1979).
2. A. J. Lichtenberg and M. A. Lieberman, *Regular and Chaotic Dynamics* (Springer-Verlag, New York, 1992, 2nd ed.).
3. G. M. Zaslavsky and R. Z. Sagdeev, *Nonlinear Physics: from the Pendulum to Turbulence and Chaos* (Nauka, Moscow, 1988; Harwood, Chur, 1988).
4. J. Green, J. Math. Phys. **20**, 1183 (1979).
5. B. V. Chirikov, Chaos, Solitons and Fractals **1**, 79 (1991).
6. J. Moser, *Stable and Random Motion in Dynamical Systems* (Princeton Univ. Press, Princeton, 1973).

7. B. V. Chirikov, E. Keil, and A. Sessler, J. Stat. Phys. **3**, 307 (1971).
8. M. Hénon and J. Wisdom, Physica D (Amsterdam) **8**, 157 (1983).
9. S. Bullett, Commun. Math. Phys. **107**, 241 (1986).
10. M. Wojtkowski, Commun. Math. Phys. **80**, 453 (1981); Ergodic Theory Dyn. Syst. **2**, 525 (1982).
11. L. V. Ovsyannikov, private communication (May, 1999).
12. V. V. Vecheslavov, Preprint IYaF 99-69 (Budker Institute of Nuclear Physics, Siberian Division, Russian Academy of Sciences, Novosibirsk, 1999).
13. V. V. Vecheslavov, Preprint IYaF 2000-27 (Budker Institute of Nuclear Physics, Siberian Division, Russian Academy of Sciences, Novosibirsk, 2000); nlin.CD/0005048.
14. V. V. Vecheslavov, Zh. Éksp. Teor. Fiz. **119**, 853 (2001) [JETP **92**, 744 (2001)].
15. V. V. Vecheslavov and B. V. Chirikov, Preprint IYaF 2000-68 (Budker Institute of Nuclear Physics, Siberian Division, Russian Academy of Sciences, Novosibirsk, 2000); Zh. Éksp. Teor. Fiz. **120**, 740 (2001) [JETP **93**, 649 (2001)].
16. L. V. Ovsyannikov, Dokl. Akad. Nauk **369**, 743 (1999).
17. I. Dana, N. W. Murray, and I. C. Percival, Phys. Rev. Lett. **62**, 233 (1989).
18. D. Sornette, L. Knopoff, Y. Kagan, and C. Vanneste, J. Geophys. Res. **101**, 13883 (1996).
19. G. Zipf, *Human Behavior and the Principle of Least Effort* (Addison-Wesley, Reading, 1949).

Translated by V. Sipachev